Scaling of H-mode Pedestal and ELM Characteristics in the JET and DIII-D Tokamaks

T.H. Osborne[1], M.N.A. Beurskens[2], L.D. Horton[3], L. Frassinetti[4], R.J. Groebner[1], A.W. Leonard[1], P. Lomas[2], I Nunes[5], S. Saarelma[2], P.B. Snyder[1], D. Zarzoso[6], I. Balboa[2], B.D. Bray[1], K. Crombé[6], J. Flanagan[2], C. Giroud[2], E. Giovannozzi[7], M. Kempenaars[2], A. Loarte[8], J. Lönnroth[9], E. de la Luna[10], G. Maddison[2], C. Maggi[3], D. McDonald[2], G.R. McKee[11], R. Pasqualotto[12], G. Saibene[13], R. Sartori[13], E. Solano[10], W. Suttrop[3], E. Wolfrum[3], M. Walsh[2], Z. Yan[12], L. Zabeo[8], and JET-EFDA[§], DIII-D, and ITPA H-mode Pedestal Study Group contributors

[1]General Atomics, PO Box 85608, San Diego, CA 92186-5608, USA
[2]EURATOM /CCFE Fusion Association, Culham Sc. Centre, Abingdon, OX14 3DB, UK
[3]Association EURATOM-Max-Planck-Institut für Plasmaphysik, D-85748 Garching, Germany,
[4]Association EURATOM-VR, Alfven Laboratory, School of Electrical Engineering, KTH, Stockholm, Sweden
[5]Centro de Fusao Nuclear, Associacao EURATOM-IST, Lisboa, Portugal
[6]CEA, IRFM, F-13108 Saint Paul-lez-Durance, France
[7]Associazione EURATOM -ENEA sulla Fusione, C.R. Frascati, Frascati, Italy
[8]ITER Organization, CS 90 046, F-13067 Saint Paul lez Durance Cedex, France
[9]Association EURATOM-Tekes, Helsinki University of Technology, Finland
[10]Associacion EURATOM-CIEMAT para Fusion, Madrid, Spain
[11]University of Wisconsin, Madison WI, USA
[12]Associazione EURATOM-ENEA sulla Fusione, Consorzio RFX Padova, Italy
[13]FUSION FOR ENERGY Joint Undertaking, 08019 Barcelona, Spain.
[§]See Appendix of F. Romanelli et al., Fusion Energy 2008 (Proc. 22nd Int Conf Geneva, 2008) IAEA, (2008)

E-mail: osborne@fusion.gat.com

Abstract. The dependence of the H-mode edge pedestal width and Type I edge localized mode (ELM) characteristics on ion gyro-radius, $\rho^*=\rho/a$, was studied in experiments combining data from the JET and DIII-D tokamaks to achieve a factor of 4 variation in ρ^* [M.N.A. Beurskens, et al., Plasma Phys. Control. Fusion (2010)]. No change was found in the radial or poloidal correlation lengths of density fluctuations in the ETB as a function of ρ^*. The ELM energy loss normalized to the pedestal energy increased with ρ^* on DIII-D to twice the value expected from an established scaling with collisionality; however, this trend was reversed on JET where the $\Delta W_{ELM}/W_{PED}$ instead decreased weakly with increasing ρ^*. The ELM size was also correlated with the proximity of the density to the value at which the power for transition from L- to H-mode is a minimum.

1. Introduction

An understanding of what sets the extent of the H-mode edge transport barrier (ETB) is a key part of developing a predictive capability for the performance of future tokamaks. For ITER to meet its design goal of Q=10, T_{PED}~4 keV is required [1]. Since the peeling-ballooning mode [2-4], sets the pressure gradient in the ETB, a model for the ETB width should allow a prediction of P_{PED}.

Extrapolation of the pedestal confinement from current devices such as JET and DIII-D to ITER is crucial to further develop the understanding of the edge confinement in ITER. For this reason a dimensionless scaling experiment has been conducted in which the normalised toroidal ion Larmor radius $\rho^* = \rho_i/a \sim (T_i^{1/2}/aB_T)^{1/2}$ at the pedestal top has been varied by a factor of four between JET and DIII-D from ρ^* = 0.002 to 0.008. ITER operates at low ρ^*

compared to JET and DIII-D and a positive dependence of the pedestal confinement on ρ^* for these two tokamaks would result in reduced global energy confinement for ITER.

At plasma-facing surfaces, particularly the divertor targets, melting and ablation limits place severe constraints on the maximum plasma energy loss per edge localized mode (ELM) in ITER. A maximum tolerable ELM energy loss limit of DW_{ELM} = 1 MJ, which corresponds to ~1% of the pedestal stored energy (W_{ped}=3/2*P_{PED}*plasma volume) has recently been set [5]. In a multi device comparison it was found that the relative ELM-size scales inversely with pedestal collisionality ($\nu^* \propto n_{ped}/T_{ped}^2$) [6]. Given the required high T_{ped}, this scaling predicts an unacceptably large ELM size, DW_{ELM}/W_{ped}>15%, for ITER; however, the physics of the ELM energy loss remains uncertain and dependencies other than ν^*, such as ρ^* cannot be ruled out.

2. Experimental Conditions for the JET-DIII-D Pedestal Comparison

JET and DIII-D are similarly shaped tokamaks with ITER-like geometries. Both devices have similar poloidal divertor configurations with JET being a factor of 1.8 larger in linear dimension than DIII-D: JET (R=2.95 m, a=0.95 m. Vol=80 m^3), DIII-D: (R=1.67 m, a=0.54 m, Vol=16 m^3). A ρ^* scan was carried out matching the aspect ratio, R/a ~ 3.2, [$(R/a)_{ITER}$ = 3.1] and cross-sectional shape in both a low triangularity configurations with δ_{upper}~0.2 and δ_{lower}~0.4 and a high triangularity configuration with δ_{upper}~0.45 and δ_{lower}~0.4. Figure 1 shows the match for the two shapes for the two devices. Generally the match is good both in triangularity and elongation, however due to the different shaping coil configuration a match in squareness was not possible.

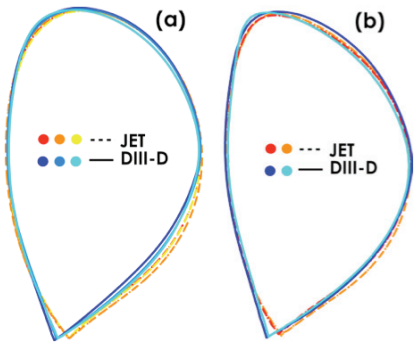

FIG. 1. Cross-sectional shapes used in ρ scan. (a) low δ, (b) high δ.*

In the dimensionless scan the gyro-radius normalized to machine size, $\rho^* \equiv 4.6\text{x}10^{-3}(m^{1/2}/z)(T_e^{ped}\ (\text{keV}))^{1/2}/(aB_T)$ was varied (where m is the atomic mass and z the atomic charge of the main ions), while seeking to keep other parameters fixed: 1) normalized pressure, $\beta^{PED} = p^{PED}/(B_T^2/2\ m_0)$, 2) safety factor, q^{PED}, 3) effective charge, Z_{EFF}, 4) ratio of electron to ion temperature, T_e/T_i, 5) ratio of toroidal velocity to sound speed, $M=10^{-4}v_T\ (m/s)/[T_i\ (ev)/m]^{1/2}$, and 6) collisionality, $\nu_e^* = 6.9\text{x}10^{-18}\ q^{PED}R^5/2a^{-3/2}Z_{EFF}\lambda_e\ n_e^{PED}\ (m^{-3})/[T_e^{PED}\ (eV)]^2$, where $\lambda_e = 3.3 - \text{Log}([n_e^{PED}\ (m^{-3})]^{1/2}/T_e^{PED}\ (eV))$ [7]. With the other dimensionless parameters matched, ρ^* varies as $\rho^* \propto a^{-5/6}B_T^{-2/3}$, and a large range in ρ^* was obtained by comparing JET discharges at B_T=2.7 T with DIII-D discharges at B_T=1 T. To maintain the other dimensionless parameters fixed in the ρ^* scan, the pedestal parameters should vary as $n_{ped} \propto (a\rho^*)^{-2}$, $T_{ped} \propto (a^{1/2}\rho^*)^{-1}$, $I_p \propto (a^{1/6}\rho^*)^{-3/2}$, and $v_T \propto (a^{1/2}\rho^*)^{-1/2}$. At the dimensionless match point where ρ^* is matched as well B_T^{DIII-D}=2.1 and B_T^{JET}=1.1. Not all of these quantities could be directly controlled and some systematic variation with respect to ρ^* occurred particularly for T_e/T_i and Z_{EFF} [Fig. 2(b,d)].

The main pedestal diagnostics are Thomson scattering for the electrons and charge exchange recombination for the ions. Details of the diagnostics as they pertain to this experiment are as given in [8]. To increase the density of measurement points in the pedestal, both tokamaks employ small sweeps of the separatrix location in the region of the pedestal measurements, and data is accumulated from the last 20%-30% of the ELM cycle for many ELMs [9,10]. At DIII-D a composite profile in normalized flux space is built from the many ELM cycles by mapping the profile from the upper outboard vertical line of sight to the outer midplane at a specific time point using the flux surface geometry of MHD equilibrium at that time. At JET the Thomson scattering line-of-sight is close to the magnetic midplane, and therefore no detailed magnetic equilibrium is required to reconstruct the midplane profiles. Instead only the radial movement of the last closed flux surface is taken into account to provide detailed midplane profiles. The extent of the ETB is set primarily by the structure of the electron temperature and density profiles since the ion temperature and carbon concentration in this region typically have relatively weak gradients. As such we use the electron profiles to obtain the pedestal top values in the discussion that follows. The ion data that are used to calculate the pedestal confinement are taken at the location of the electron pedestal top as obtained by fitting a modified hyperbolic tangent function (*mtanh*) [11] to the electron data.

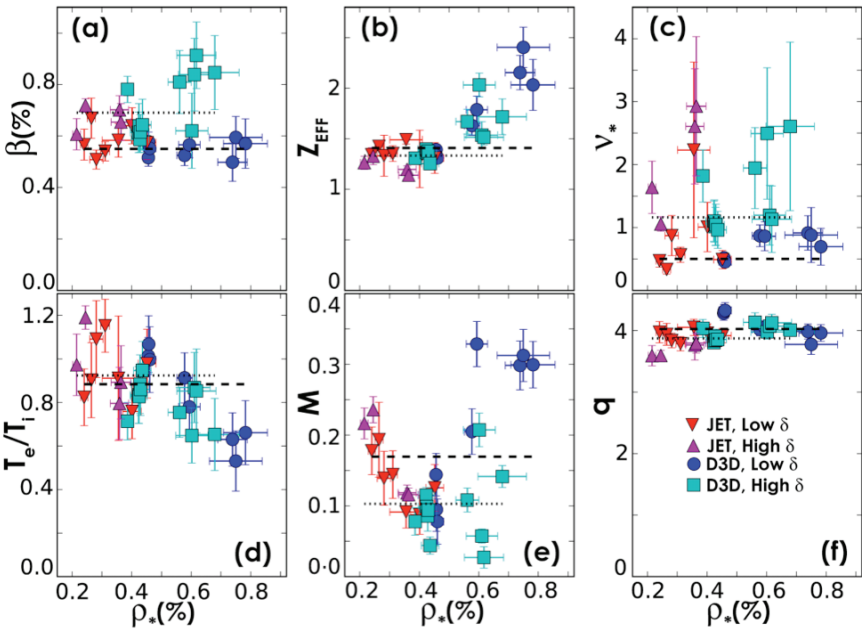

FIG. 2. Variations in pedestal dimensionless parameters through the ρ scan. (a) normalized pressure β, (b) effective charge Z_{EFF}, (c) electron collisionality ν_*, (d) electron to ion temperature ratio, (e) toroidal velocity over sound speed M, (f) safety factor q. Data for both JET (red and magenta points) and DIII-D (blue and cyan points) in both the high and low triangularity shapes of Fig. 1 are shown. Horizontal dashed and dotted lines represent averages for the low and high triangularity data respectively.*

3. Pedestal Scaling

For all plasmas in the ρ* experiment, the ratio of the pedestal to total stored remained relatively fixed at between 30% and 40% [Fig. 3(a)]. This is perhaps indicative of the effect of pedestal pressure on global energy confinement through profile stiffness. This indicates not only the importance of exploring the scaling of pedestal pressure based on local parameters but also the possible applicability of scaling laws developed for overall stored energy to the pedestal. Examining the ITER physics base overall energy confinement scaling, $H98_{y,2}$ we find a small degradation towards ρ* in JET [Fig. 3(b).

It is possible to look for evidence of ρ^* effects on the pedestal by comparing the pedestal pressure to published scaling laws as a function of ρ^*. In these comparisons we add DIII-D data covering a range of pedestal β values and discharge shapes [12], including data from DIII-D ITER demonstration discharges, to the ρ_* scan results. We compare to two models based on fitting to a large number of discharges from the ITPA H-mode database [13] [Figs 3(a,b)]. The first of these is a thermal conduction model which assumes that the pedestal stored energy is governed by an energy confinement time which scales with global parameters similarly to the overall energy confinement (Eq. w_{PED2} in [13]),

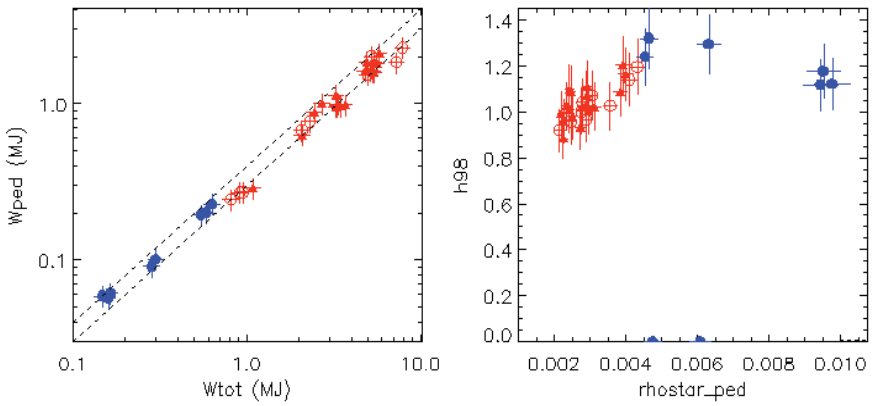

FIG. 3. (a) Pedestal versus total confinement and (b) H98y vs ρ^* for the JET (red) and DIII-D (blue) ρ^* experimental data, triangles for high and circles for low δ pulses.

$$p^{\text{CORDEY-THERMAL}}\,(\text{kPa}) = 8.1 I_P\,(\text{MA})^{1.41} R^{1.37} P\,(\text{MW})^{0.5} n\,(10^{19}/\text{m}^3)^{-0.15} B_T^{0.32} \text{m}^{-2} F_q^{1.67} \kappa^{1.21}/(1.5\ V),$$

where all units are MKS except where noted, and P is the heating power, n the line average density, m the atomic mass, F_q the ratio of q at the 95% flux surface, q_{95}, to the cylindrical q, $q_{CYL}=5\kappa a^2 B_T/RI_P$ (MA), κ is the elongation, and V is the plasma volume [Fig. 4(a)]. This model fits the data well with little indication of a residual ρ^* dependence: $p/p^{\text{MODEL}} \propto (\rho^*)^{0.2}$.

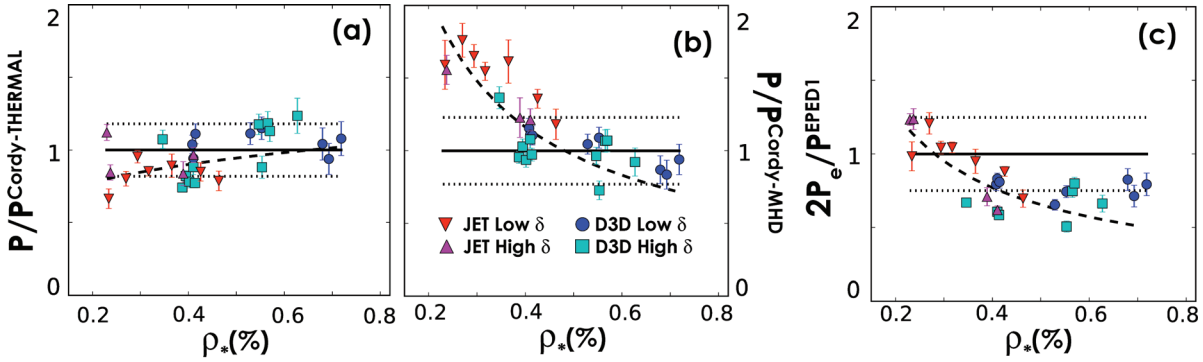

FIG. 4. Comparison to pedestal models as a function of ρ^* (a) Thermal conduction model for pedestal pressure based on global parameters, (b) MHD model for pedestal pressure based on local pedestal dimensionless parameters, (c) EPED1 model for pedestal pressure. Dotted lines represent model uncertainties. Dashed lines are fits to a power of ρ^*.

The uncertainty in the model shown in Figs 4(a,b) is the quoted RMS deviation of the ITPA database data from the model. The second pedestal pressure scaling [Fig. 4(b)], Eq. (4) in [13]) is again based on fitting to the ITPA H-mode database but using local pedestal dimensionless parameters,

$$p^{\text{CORDEY-MHD}}\,(\text{kPa}) = 0.83\,\rho_{ped}^{0.27}\,\nu_{ped}^{-0.8}\ \text{m}^{0.2} F_q^{2.29} \varepsilon^{-2.56} \kappa^{2.48}\,[RI_P\,(\text{MA})^2]/(1.5\ V)$$

where $\rho_{ped} \equiv T_{av}$ (keV)$^{1/2}$/I_p (MA), $T_{av} = (T_e+T_i)/2$, $\nu_{ped} \equiv n_e^{ped}$ (10^{19} m^{-3}) R/T_{av}^2, $\varepsilon=(a/R)$. This model shows a significant residual ρ^* dependence outside of its uncertainty of $p/p^{MODEL} \propto (\rho^*)^{-0.8}$.

The EPED1 model predictions for pedestal pressure are shown in Fig. 4(c). The pressure measurments are in agreement with the model predictions within uncertainties of the model and the data. Also here a residual ρ^* dependence is possibly indicated in the EPED1 results, of $p/p^{MODEL} \propto (\rho^*)^{-0.7}$, although only the ρ^* scan data appear to show the effect and this is mostly a contrast between the JET and DIII-D data; the DIII-D data systematically lie below the predictions of EPED1 by ~40%-50%, whereas the JET data shows a decrease of $2*p_e/p_{EPED1}$ with ρ^*.

4. Effect of ρ_* on Pedestal Turbulence

At DIII-D, an examination of the correlation lengths of density fluctuations in the ETB using the beam emission spectroscopy (BES) diagnostic has been performed [14]. The BES system was set to measure the characteristics of long-wavelength ($k_\perp \rho_I < 1$) density fluctuations in the pedestal region for the lower triangularity discharges of the ρ^* scan. The radial correlation length of the fluctuations was determined using a 5x6 array of discrete channels covering an approximately 4.5x7 cm region near the outboard midplane at 0.9<r/a<1.0 [Fig. 5(a)]. The radial correlation length is taken as the characteristic decay length of the radial correlation function, which was integrated over the observed broadband fluctuations (50-150 kHz). The radial correlation function is shown in Fig. 5. It exhibits a correlation length of ~1.5–2 cm (~w_{Te}), and is found to be largely independent of the ρ^*.

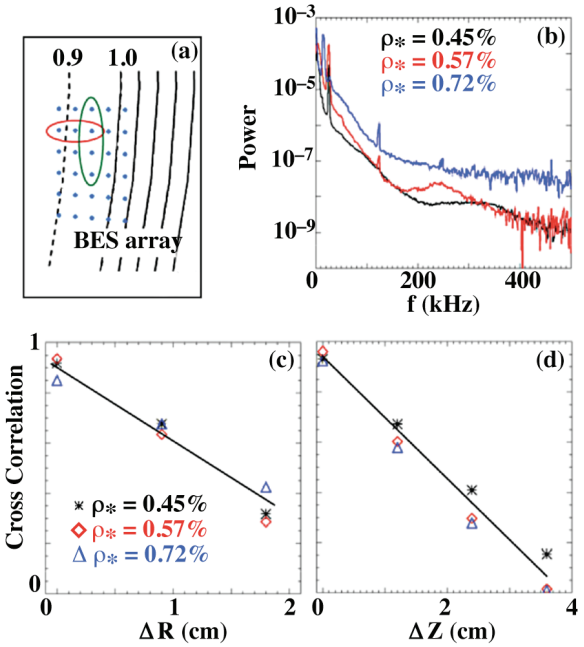

FIG. 5. Beam emission spectroscopy measurements in the pedestal region. (a) geometry of BES measurement points covering the ETB region 0.9< ψ_N < 1, (b) power spectrum as a function of ρ (c) frequency integrated cross correlation as a function of radial position (d) frequency integrated cross correlation as a function of vertical (poloidal) position.*

5. ELM Characteristics

The energy loss at Type I ELMs, ΔW_{ELM}, normalized to the pedestal energy, $W_{PED} = 3/2 p_{PED} V$, increased strongly with ρ^* in DIII-D discharges as shown in Fig. 6. The ELM energy loss was measured by computing the change in the stored energy by integrating the total pressure profiles before and after an ELM over the plasma volume (averaged over many ELMs) (open points, Fig. 6), and from magnetic measurements (solid point, Fig. 6). The increase in ELM losses with ρ^* on DIII-D is also evident in the conductive and convective parts of the pedestal pressure change. The trend of increasing ELM losses with ρ^* does not continue to lower ρ^* through the JET discharges, which show a slightly decreasing trend with ρ^*.

A comparison of $\Delta W_{ELM}/W_{PED}$ to an established scaling [6] with collisionality is shown in Fig. 6(b). Most data in the ρ^* scan lie within the range of previous data from a number of

tokamaks (gray area in Fig. 6(b); however, the large ρ^* DIII-D data at low triangularity significantly exceeds what would be expected for its collisionality.

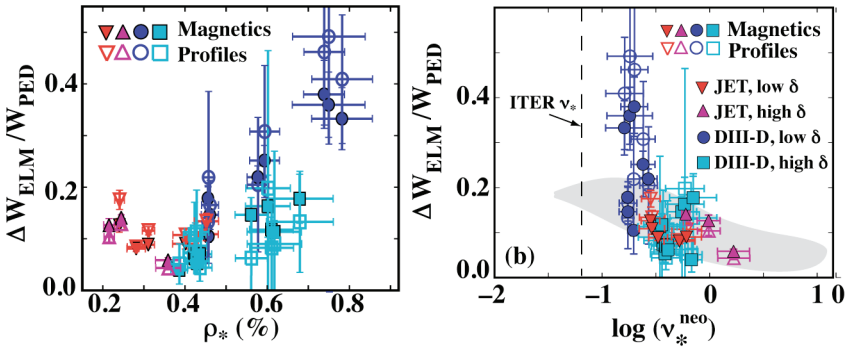

FIG. 6. (a) Changes in Type I ELM energy loss normalized to pedestal energy as a function of ρ. Scalings for Type I ELM energy loss, $\Delta W_{ELM}/W_{PED}$, for ρ* scan discharges. (b) $\Delta W_{ELM}/W_{PED}$ versus collisionality, previous data for several tokamaks is shown in the gray region [Loarte-2003].*

$\Delta W_{ELM}/W_{PED}$ has been noted to increase as the heating power, P_{HEAT}, is reduced to near the threshold power for transition into H-mode, P_{LH}. The L- to H-mode threshold power was not measured in the ρ^* scan discharges, however the high ρ^* DIII-D discharges are nearly a factor of 4 above the standard threshold power scaling [15]. This scaling however only applies to the higher density regime where the threshold power increases with density. Below a certain critical density, $n_{e\text{-}min}$, the opposite is true and the threshold power increases as the density is reduced. The scaling of $n_{e\text{-}min}$, as well as the scaling of P_{LH} with $n_e<n_{e\text{-}min}$ are not well established, but using nominal values of $3.1\text{x}10^{19}\text{m}^{-3}$ for DIII-D and $1.8\text{x}10^{19}\text{m}^{-3}$ for JET as given in [15] shows an apparent correlation between the large $\Delta W_{ELM}/W_{PED}$ at large ρ^* on DIII-D and proximity to $n_{e\text{-}min}$. If the large ρ^* DIII-D discharges have $n_e<n_{e\text{-}min}$, it is possible that P_{HEAT} is much closer to P_{LH} than given by the P_{LH} scaling valid in the $n_e>n_{e\text{-}min}$ regime.

There is some increase in the amplitude (δB/B) and duration of the magnetic fluctuations during the Type I ELMs with increased $\Delta W_{ELM}/W_{PED}$ at large ρ^* on DIII-D. The duration increase is particularly significant when normalized to the overall energy confinement time, which decreases with increasing ρ^*. However there is no other obvious change in the characteristics of the magnetic fluctuations and the ELMs at large ρ^* do not appear to become compound.

6. Pedestal Structure Analysis

An extensive study has been conducted on the scaling of the pedestal width of the electron kinetic pedestal profiles between JET and DIII-D as a function of ρ*. Primary sources of error in the electron data are: 1) irreproducibility of the ELM cycle (the ELM cycle may be naturally non-periodic), 2) the finite extent of the inter-ELM period chosen for data selection, 3) noise on the Thomson scattering diagnostic (primarily photon and detector dark current noise), 4) calibration error in the Thomson scattering diagnostic, 5) error in equilibrium reconstruction used to accumulate many TS pulses into a single profile resulting in a positional uncertainty in the data points. 6) uncertainties in the instrument spatial resolving power across the pedestal region.

Lack of reproducibility of the ELM cycle and uncertainties in the TS calibration are the primary sources of value error in the DIII-D data, while TS system noise typically dominates the JET data. Error bars for the experimental values are estimated by examining the quality of the fit in the region at the top where positional uncertainty is unimportant. A positional error is then assigned to give reduced $\chi^2=1$ over the entire range of the fit. Errors are propagated through to the coefficients defining the profile characteristics with the positional uncertainties included through orthogonal distance regression [16]. The pedestal parameters are

determined by fitting to a modified hyperbolic tangent function (*mtanh*) [11] in the edge region.

As discussed in [8] the spatial resolution of the Thomson scattering systems, set by the view solid angle and the extent of the TS laser beam, must be taken into account in the analysis of the pedestal structure. In principle the deconvolution with the instrument kernel should take place on the spectral data form the Thomson scattering polychromator [17]. This deconvolution can be approximated by a forward convolution as:

$$n_e^{\text{Measured}} = n_e^{\text{dev}} \otimes I^{\text{kernel}} \tag{1a}$$

$$T_e^{\text{Measured}} = \left[\frac{\left(\sqrt{T_e^{\text{dev}}} \times n_e^{\text{dev}} \right) \otimes I^{\text{kernel}}}{\left(n_e^{\text{dev}} \otimes I^{\text{kernel}} \right)} \right]^2 \quad . \tag{1b}$$

Where the superscript *dcv* indicates the deconvolved *mtanh* fits to the profiles, I^{kernel} is the instrument kernel. Note that reconstructing the deconvolved T_e profiles is not through a straight forward deconvolution but requires weighting of the kernel by the density profile to reflect the number of photons received per spatial element. Both the DIII-D and JET pedestal profiles have been analysed by applying the forward deconvolutions in equation (1) to the profiles. For most of the JET data discussed here, the computed true pedestal width is significantly smaller, 40%-70%, than the observed value e.g. Fig. 8, while for DIII-D there is a relatively small correction, <10 %.

8. Conclusions

By combining data from JET and DIII-D, up to a factor of 4 variation in ρ^* was achieved. In these discharges the total stored energy was proportional to the pedestal stored energy. Comparison to theory-based scalings expressed in terms of local pedestal parameters suggests an inverse dependence of pedestal pressure on ρ^*. This is a positive result for ITER which will operate at smaller ρ^* than existing tokamaks. Comparison of the ρ^* variation discharges with a pedestal pressure scaling based on global parameters similar to the overall confinement scaling, gave little indication of residual ρ^* dependence. This result is perhaps expected due to the link between core and pedestal confinement.

Whether the unexpectedly large value of $\Delta W_{ELM}/W_{PED}$ in the high ρ^* DIII-D discharges is a consequence of the ρ^* value itself or some other characteristic of these discharges remains unclear. These discharges lie near, or perhaps below, the density at which the H-mode threshold power begins to increase as the density is reduced. As such, the proximity of these discharges to the H-mode power threshold cannot be determined without a direct measurement. If the large $\Delta W_{ELM}/W_{PED}$ were a consequence of large ρ^* or a proximity to this critical density then this will not be a concern for ITER since it will operate at small ρ^* and there are indications the $n_{e\text{-min}}$ decreases with increasing machine size [Martin-2008] and already $n_{e\text{-min}}$ on JET it is well below the ITER operating density.

This work was supported in part by the US Department of Energy under DE-FC02-04ER54698 and DE-FG02-89ER53296 and was partly funded jointly by the UK Engineering and Physical Sciences Research Council and by the European Communities under the contract of Association between EURATOM and UKAEA. It was carried out within the framework of the European Fusion Development Agreement. The views and opinions expressed herein do not necessarily reflect those of the European Commission.

References

[1] KINSEY, J.E., et al., Phys. Plasmas **9** (2002) 1676
[2] WILSON, H.R., et al., Phys. Plasmas **9** (2002) 1277
[3] SNYDER, P.B., et al., Phys. Plasmas **9** (2002) 2037
[4] SAARELMA, S., et al., Plasma Phys. Control. Fusion **51** (2009)
[5] ZHITLUKIN, et al., J. Nucl. Mater. **363–365** (2007) 301–307
[6] LOARTE, A., et al., Plasma Phys. Control. Fusion **45** (2003) 1549–1569
[7] SAUTER, O., et al., Phys. Plasmas **6** (1999) 2835
[8] BEURSKENS, M.N.A., et al., Plasma Phys. Control. Fusion (2009 or 2010)
[9] BEURSKENS, M.N.A., et al., Nucl. Fusion **48** (2008) 095004
[10] FENSTERMACHER, M.E., et al., Nucl. Fusion **45** (2005) 1493–1502
[11] GROEBNER, R.J., et al., Plasma Phys. Control. Fusion **44** (2002) A265–A272
[12] SNYDER, P.B., et al., Phys. Plasmas **16** (2009) 056118
[13] CORDEY, J.G., et al., Nucl. Fusion **43** (2003) 670-674
[14] McKEE, G.R., et al., Plasma Fusion Research **2** (2007) 21025.
[15] MARTIN, Y. and ITPA threshold database working group, J. Phys.: Conf. Series **123** (2008) 12033.
[16] BOGGS, P.T., et al., National Inst. of Standards and Tech. Report NISTIR 92-4834 (June 1992).
[17] SCANNELL, R. PhD thesis; Investigation of the H-mode Edge Profile Behaviour on MAST using Thomson Scattering, University of Cork, Ireland (2007)